Journal of Alloys and Compounds 983 (2024) 173923

Contents lists available at ScienceDirect

Journal of Alloys and Compounds

journal homepage: www.elsevier.com/locate/jalcom

Electrocaloric effect near room temperature in lead-free Aurivillius phase $Sr_2Bi_4Ti_5O_{18}$ upon La and Nb codoping

Sara Lafuerza [a,b,*], David Gracia [a,b], Javier Blasco [a,b], Marco Evangelisti [a,b]

[a] Instituto de Nanociencia y Materiales de Aragón (INMA), CSIC-Universidad de Zaragoza, Zaragoza 50009, Spain
[b] Departamento de Física de la Materia Condensada, Universidad de Zaragoza, C/ Pedro Cerbuna 12, Zaragoza 50009, Spain

ARTICLE INFO

Keywords:
Electrocaloric effect
Aurivillius phases
Lead-free ferroelectrics
Direct and indirect electrocaloric measurements

ABSTRACT

La and Nb codoping of ferroelectric five-layer Aurivillius phase $Sr_2Bi_4Ti_5O_{18}$ ($T_C \sim 560$ K), induces compositional disorder and diffuse relaxor transitions at much lower temperatures than the parent compound, while preserving the orthorhombic structure. For moderate La and Nb concentrations, the ferroelectric properties are enhanced in the vicinity of room temperature, and so is the electrocaloric effect as measured directly with a homemade quasi-adiabatic calorimeter. The adiabatic temperature change reaches, e.g., in $Sr_2Bi_{3.44}La_{0.5}Ti_{4.8}Nb_{0.2}O_{18}$, $\Delta T \sim 0.3$ K at 355 K with a temperature span ~ 15 K, under $\Delta E = 37$ kV/cm. Besides, a large field dispersion of the electrocaloric effect is found, ascribed to field-induced transitions from short-range-ordered relaxor to long-range-ordered ferroelectric states. Indirect estimations of the electrocaloric effect from electric polarization data are not able to quantitatively predict the direct results and emphasize the need of applying direct measurement methods, especially for relaxor ferroelectrics.

1. Introduction

Solid-state caloric effects are among the most promising alternatives to vapor-compression technology for refrigeration and heat pump applications near room temperature [1,2]. Besides the avoidance of harmful gases, the main gain of solid-state cooling and heating is the higher energy efficiency, which translates into a significant reduction in electricity consumption [3]. The electrocaloric effect (ECE) is defined as the reversible adiabatic temperature (ΔT) and isothermal entropy (ΔS) variations exhibited by dielectrics when an electric (E) field is cyclically applied and removed [4–7]. It maximizes at temperatures near the Curie temperature (T_C) of paraelectric to ferroelectric phase transitions, where ΔS is enhanced [8]. The ECE is advantageous over the magnetocaloric and barocaloric effects because E fields are much easier to apply than high magnetic fields or pressures, respectively [9,10]. It should be mentioned that there is no standardized ECE measurement system nor method. The existing approaches fall into two categories, direct and indirect methods [11]. The former directly measure either ΔT or the released heat in the material, while the latter rely on the measurement of the change in the electric polarization as a function of temperature and E field, to which thermodynamics formulations based on Maxwell relations are applied. Only a few groups have developed setups dedicated to direct measurements, being the indirect methods the most commonly used, as they are faster and simpler, however they involve several limitations and might be unreliable [10,11].

Aurivillius phases are ferroelectrics recognized as promising electrocaloric (EC) candidates [10]. They are composed by a number n of perovskite-like layers $(A_{n-1}B_nO_{3n+1})^{2-}$ sandwiched between bismuth oxide layers $(Bi_2O_2)^{2+}$ along the crystallographic c-axis (Fig. 1). The high-temperature crystal structure in the paraelectric phase is tetragonal (space group *I4/mmm*) and complex polar structures (either orthorhombic or monoclinic) involving not only the B-cation like in simple perovskites, but also the A-cation and oxygens, originate below T_C [10]. They feature a large compositional and structural flexibility to accommodate a wide range of A and B cations. A number of compositions, such as $Bi_{3.25}La_{0.75}Ti_{12}O_3$ [12] and $Bi_2A_{n-1}B_nO_{3(n+1)}$ with A = Sr/Bi, B = Ta/Nb and n = 2, 4 [13], were found to have high dielectric strength, low leakage current and strong resistance to electrical fatigue, characteristics associated to the presence of the bismuth oxide layers that make them highly potential EC materials. Nevertheless, a drawback for widespread EC refrigeration applications near room temperature is that these compounds generally show too high T_C values, e.g., large ΔT found at $T_C \sim 560$ K for $SrBi_2Ta_2O_9$ thin films [14]. Hence, the challenge with Aurivillius phases is lowering T_C towards room temperature while

* Corresponding author at: Instituto de Nanociencia y Materiales de Aragón (INMA), CSIC-Universidad de Zaragoza, Zaragoza 50009, Spain.
E-mail address: lafuerza@unizar.es (S. Lafuerza).

https://doi.org/10.1016/j.jallcom.2024.173923
Received 27 October 2023; Received in revised form 8 February 2024; Accepted 18 February 2024
Available online 20 February 2024

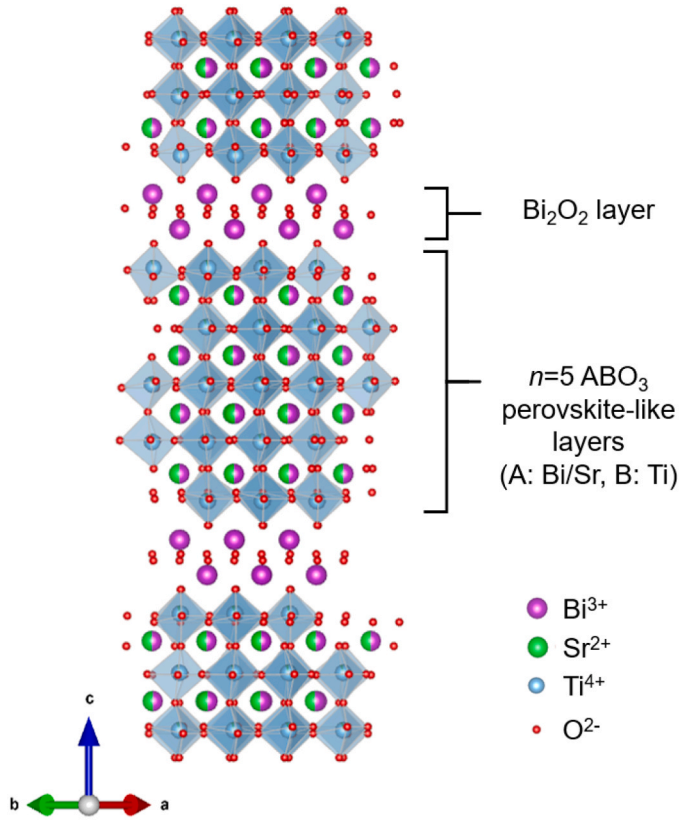

Fig. 1. Orthorhombic crystal structure (*B2cb* space group) of five-layer Aurivillius phase $Sr_2Bi_4Ti_5O_{18}$ at room temperature. The structure is nearly tetragonal with $a \sim b$. Figure prepared with VESTA [27].

maintaining the excellent dielectric properties. Doping strategies have been reported to decrease T_C, namely, A-site substitution with divalent cations (Ba^{2+}, Sr^{2+}) and/or lanthanides [15–20], and B-site substitution with an appropriate choice of pentavalent cations (Ta^{5+}, Nb^{5+}) [18,21,22]. At the same time, the introduction of structural disorder through chemical substitutions in ferroelectrics induces diffuse phase transitions which can be useful to expand the working temperature range of these materials as refrigerants [10,23,24]. Besides, above critical concentrations, chemical substitutions can lead to relaxor behavior, where instead of long-range ferroelectric domains, the strong compositional and structural disorder yields the formation of polar nanoregions with randomly distributed directions of dipole moments [25,26]. The EC properties of a few Aurivillius phases with different chemical substitutions bringing T_C closer to room temperature and exhibiting relaxor behavior were surveyed [17–20]. Direct ECE measurements in either Pr^{3+} or Ba^{2+} doped $SrBi_2(Nb_{0.2}Ta_{0.8})_2O_9$ showed ΔT values $\sim$ 0.5 K and $\sim$ 0.8 K respectively, although no clear ECE peak was obtained in the temperature range around their T_C [17–19]. Besides, in Pr^{3+} doped $SrBi_2(Nb_{0.2}Ta_{0.8})_2O_9$, a strong disagreement between the direct and indirect ECE measurements was reported [18]. Much smaller ΔT values were reported from indirect ECE estimations in $SrBi_{1.98}La_{0.02}Nb_{2-x}Ta_xO_9$ [20].

Despite the expectations placed on Aurivillius phases as EC materials, the scarce dedicated studies performed so far are limited to compounds with Nb and/or Ta at the B-site. A potentially interesting lead-free Aurivillius family where B = Ti is $Sr_{n-3}Bi_4Ti_nO_{3n+3}$, whose T_C decreases as n increases, being 950, 790 and 560 K for n = 3, 4 and 5, respectively [28]. We focus on five-layer $Sr_2Bi_4Ti_5O_{18}$ (n = 5), with the lowest T_C and a very abrupt ferroelectric transition [28,29]. La^{3+} substitution for Bi^{3+} at the A-site in $Sr_2Bi_{4-x}La_xTi_5O_{18}$ was reported to promote a relaxor ferroelectric behavior for $x \geq 0.5$ and yielded T_C values near room temperature but with very diffuse character and thus low electric permittivity and polarization values [29]. Inspired by results on the ferroelectric properties of $Bi_4Ti_3O_{12}$ (n = 3) [30,31], we follow a strategy that combines A-site doping (Bi^{3+} replacement by La^{3+}) with additional B-site doping substituting Ti^{4+} by Nb^{5+}. Herein, we report the effects of such La/Nb codoping on the crystal structure, electrical and EC properties of lead-free Aurivillius phase $Sr_2Bi_4Ti_5O_{18}$. To preserve the charge balance, given the heterovalent B-site substitution (Ti^{4+} replaced by Nb^{5+}), Bi vacancies are formed in the compositions with general chemical formula $Sr_2Bi_{4-x-1/3y}La_xTi_{5-y}Nb_yO_{18}$ (SBLTN-x/y). The ECE is determined in the optimum compositions from direct measurements using a homemade quasi-adiabatic calorimeter and complemented further by indirect estimations from the electric polarization data at several temperatures. The codoped composition $Sr_2Bi_{3.44}La_{0.5}Ti_{4.8}Nb_{0.2}O_{18}$ (SBLTN-0.5/0.2), which features a modest relaxor ferroelectric behavior, shows the best EC performance with a maximum $\Delta T \sim$ 0.3 K at 355 K and temperature span $\sim$ 15 K, under ΔE = 37 kV/cm. The best composition in terms of the closest proximity of the ECE to room temperature is $Sr_2Bi_{3.41}La_{0.5}Ti_{4.7}Nb_{0.3}O_{18}$ (SBLTN-0.5/0.3), with a maximum $\Delta T \sim$ 0.2 K at 325 K and temperature span $\sim$ 16 K, under the same ΔE. Moreover, the comparison between the direct and indirect ECE results evidences that the indirect method must be used with caution since it fails to reproduce the ECE peak magnitude as a function of the E field increase and also its temperature span. These results reinforce the importance of using direct ECE measurements for a truly reliable EC characterization and successful discrimination of future potential refrigerant materials.

2. Experimental details

The studied polycrystalline samples of five-layer Aurivillius compounds $Sr_2Bi_{4-x-1/3y}La_xTi_{5-y}Nb_yO_{18}$ (SBLTN-x/y) can be divided into two series: A-site La doped SBLTN-x/0 with x = 0, 0.25, 0.5, 0.6; and A-site La doped (x = 0.5) together with B-site Nb doped (i.e., La/Nb codoped) SBLTN-0.5/y with y = 0.1, 0.2, 0.3, 0.4. The SBLTN-x/y samples were prepared by the standard solid-state reaction method and their crystal structures were characterized by powder X-ray diffraction (XRD) at room temperature in a Rigaku D-Max system using Cu $K\alpha_{1,2}$ wavelengths. Precursor powders of Bi_2O_3, La_2O_3, $SrCO_3$, TiO_2 and Nb_2O_5 with purities not less than 99.9% were used. An excess of Bi_2O_3 (3–5 wt%) was applied to compensate for the bismuth losses during sintering due to its strong volatility. The stoichiometric mixture (with the mentioned Bi_2O_3 excess) was mixed and ground in a ball mill for 2 h. The powders were then calcined at 850 ºC for 4 h. The resulting products were reground, pressed into pellets and sintered at 1190 ºC for 4 h. After this step, SBLTN-x/0 samples are single phase but La/Nb codoped SBLTN-0.5/y samples show additional intermediate phases ($SrTiO_3$ perovskite and $SrBi_2Ti_4O_{15}$ phases). In this case, the last step is repeated until the XRD patterns no longer show progress in the chemical reaction. In the end, all the samples are single phase except SBLTN-0.5/y with y = 0.3 and 0.4 that have tiny impurities of a pyrochlore phase ($\approx$ 1 wt%). Rietveld analysis of the X-ray patterns was performed using the Fullprof package program [32].

Electrical and EC properties measurements were conducted on sintered disc-shaped samples, with typical dimensions of 8 mm diameter and thickness between 0.5 and 1 mm. Electrodes were made with silver paste in sandwich geometry. The relative electric permittivity was derived from measurements with an impedance analyzer (Wayne Kerr Electronics 6500B), applying sinusoidal excitations of 1 V amplitude at several frequencies between 100 Hz and 4 MHz. Temperature dependent measurements were carried out in a homemade sample insert placed inside a tubular furnace. Both heating and cooling ramps with a typical velocity value of 1 K/minute were applied. The polarization versus electric field $P(E)$ curves were recorded using a commercial polarization analyzer (aixACCT Easy Check 300) jointly with a high voltage amplifier (Trek 610E), applying sinusoidal excitations with

typical frequency of 10 Hz and E field amplitudes up to 60−70 kV/cm. $P(E,T)$ curves as a function of temperature were measured in a home-made sample holder with a heater, being the samples immersed in silicon oil to prevent electric discharges at high voltages. For the evaluation of the ECE, both direct and indirect methods have been used. Direct measurements were performed using a dedicated in-house-developed quasi-adiabatic calorimeter. The adiabatic temperature change ΔT was measured as a function of temperature every 1 K and at different applied E field variations ΔE. Samples were measured in the "contactless" mode to minimize heat losses, held only by the high voltage coaxial cable and a K-type thermocouple for the direct measurement of ΔT. Voltages up to either 2 kV or 5 kV were applied using two different homemade high-voltage converters. Further description of the quasi-adiabatic calorimeter measurements can be found elsewhere [33]. For the indirect estimation, well-known thermodynamic formulations based on Maxwell relations have been applied to the $P(E,T)$ data to derive ΔS as a function of temperature. To further deduce ΔT from ΔS, we performed heat capacity (c_p) measurements using a Quantum Design PPMS on thin pressed pellets (ca. 4 mg) of polycrystalline samples, thermalized by ca. 0.2 mg of Apiezon H grease, whose contribution was subtracted by using a phenomenological expression. Finally, density (ρ) measurements were conducted by the conventional Archimedes' method.

3. Results and discussion

3.1. Structural characterization

Fig. 2 compares the XRD patterns of selected $Sr_2Bi_{4-x-1/3y}La_xTi_{5-y}Nb_yO_{18}$ (SBLTN-x/y) samples. Although all the compositions show a pseudotetragonal symmetry because of the very similar a and b lattice parameters, the best refinements of the X-ray patterns are obtained using an orthorhombic structure with *B2cb* space group [34], which is the structure of the parent compound (Fig. 1). Table 1 summarizes the refined lattice parameters and Figures S1-S4 show the Rietveld refinements for representative compositions.

In La doped SBLTN-x/0 series, substitution of Bi for La gives rise to a unit cell shrinkage that is especially observed on the c-axis. This result must be ascribed to the smaller size of La^{3+} with respect to Bi^{3+} as tabulated in [35] (note that in this ref. only 8-fold coordinated cations can be directly compared). Competitive effects in the unit cell seem to exist in the La/Nb codoped SBLTN-0.50/y series. In this case, Ti^{4+} is replaced by Nb^{5+}, which has a larger ionic radius (0.605 and 0.64 Å, respectively) [35] and, simultaneously, vacancies are formed at the Bi sublattice, while keeping constant a moderate amount of La ($x = 0.5$). Overall, the unit cell volume seems to expand upon Nb doping but the behaviour is non-isotropic. The lattice parameters of the *ab*-plane continuously increase, which is likely related to the increase in Nb content (y). Besides, the c-axis first decreases for $y \leq 0.2$, then it expands for higher substitution values ($0.3 \leq y \leq 0.4$).

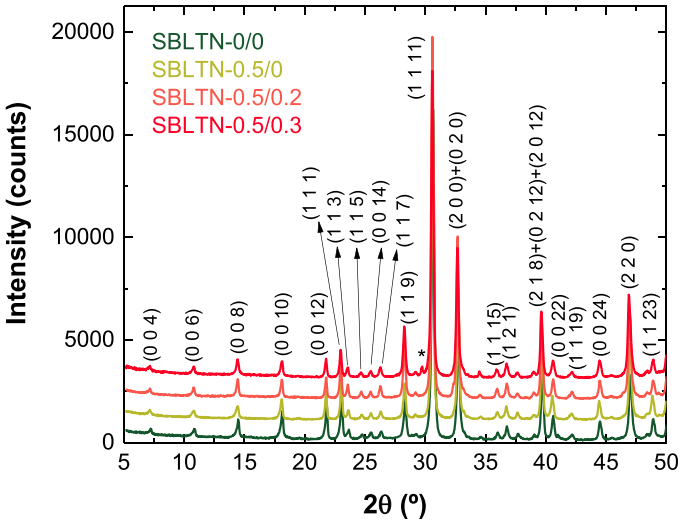

Fig. 2. X-ray diffraction patterns of SBLTN-0/0, SBLTN-0.5/0, SBLTN-0.5/0.2 and SBLTN-0.5/0.3 at room temperature with the indexation of the main diffraction peaks of the orthorhombic structure with *B2cb* space group. The asterisk (*) marks the main peak of the pyrochlore phase tiny impurity (≈ 1 wt %) in SBLTN-0.5/0.3.

3.2. Electrical properties

Fig. 3 shows the relative electric permittivity ε_r collected at 50 kHz as a function of temperature for various samples of La doped SBLTN-x/0 and La/Nb codoped SBLTN-0.5/y series, while the characteristic parameters of each sample are summarized in Table 2. This comparison allows for a sample screening in terms of the transition temperature and sharpness. The abrupt peak in the ferroelectric parent compound SBLTN-0/0, increasingly shifts to lower temperatures and becomes smoother in the La doped compositions when x rises (Fig. 3(a)), in agreement with previous reports [15,29]. Although transition temperatures at or near room temperature are obtained upon La doping, this is achieved at the expense of making the transition extremely diffuse with very low permittivity values. Interestingly, adding Nb doping to the $x = 0.5$ La doped compound (SBLTN-0.5/0) allows lowering further the transition temperature, while regaining some sharpness as illustrated by the results for the SBLTN-0.5/y series (Fig. 3(b)). We note that with respect to SBLTN-0.5/0, the maximum value of the electric permittivity ε_m increases to approximately double in the $y = 0.1$ compound, still grows a bit in $y = 0.2$ and then seems to saturate as the value is similar for $y = 0.3$.

The permittivity measurements for the La/Nb codoped samples reveal additional features of the transition. Fig. 4 shows the relative electric permittivity of SBLTN-0.5/0.2, collected at 50 kHz on heating and cooling, as well as at several other frequencies between 100 and 4 MHz on heating. The temperature of the maximum of the relative electric permittivity T_m shows a difference of about 10 K between the heating and cooling curves (Fig. 4(a)), a significant thermal hysteresis suggestive of a first-order transition. Besides, upon increasing the frequency, T_m shifts to higher temperatures together with a decrease in ε_m (Fig. 4(b)), as typically found in relaxor ferroelectrics [25]. The temperature dispersion between T_m values determined by frequencies differing by four orders of magnitude (100 Hz – 100 kHz) is indicated as ΔT_m in Table 2 for each sample. In La doped SBLTN-x/0, ΔT_m increases with x, reaching a maximum value $\Delta T_m = 8$ K for $x = 0.6$. Then, the value $\Delta T_m = 4$ K for the $x = 0.5$ sample, in good agreement with previous measurements [29], slightly decreases upon Nb doping in the SBLTN-0.5/y series. We find that ΔT_m is considerably lower in our SBLTN-x/y compositions than in related Aurivillius relaxor ferroelectrics, e.g., ΔT_m (500 Hz – 500 kHz) ~ 30–70 K for two-layer $Sr_{1-x}Ba_xBi_2Nb_2O_9$ [36], ΔT_m (1 kHz – 1 MHz) ~ 20 K for four-layer $BaBi_4Ti_4O_{15}$ and ΔT_m (1 kHz – 1 MHz) ~ 30–40 K for five-layer $Ba_2Bi_4Ti_5O_{18}$ [25]. This indicates a relatively modest relaxor character of SBLTN-x/0, which is further weakened by the addition of Nb in SBLTN-x/y.

Both La doped SBLTN-x/0 and La/Nb codoped SBLTN-0.5/y compositions show a typical ferroelectric-like hysteresis in the $P(E)$ curve at room temperature (Fig. S5), being the evolution of the ferroelectric polarization values upon doping in consistency with the electric permittivity results as described next for representative compositions. The polarization (both the value at maximum E field P_{max} and the remanent polarization P_r) of the parent compound SBLTN-0/0 strongly decreases in La doped SBLTN-0.5/0, and then it is substantially restored in La/Nb codoped SBLTN-0.5/0.2 (Fig. 5 and Table 3). Besides, the polarization switching coercive field E_C decreases only slightly upon La doping while a further reduction is gained by adding Nb. The

Table 1
Refined lattice parameters for $Sr_2Bi_{4-x-1/3y}La_xTi_{5-y}Nb_yO_{18}$ (SBLTN-x/y) using an orthorhombic structure with *B2cb* space group.

SBLTN-x/y	Composition	a (Å)	b (Å)	c (Å)	Vol. (Å^3)
0/0	$Sr_2Bi_4Ti_5O_{18}$	5.4625(9)	5.4632(9)	48.8804(16)	1458.7(3)
0.25/0	$Sr_2Bi_{3.75}La_{0.25}Ti_5O_{18}$	5.4628(9)	5.4627(9)	48.8264(25)	1457.1(4)
0.5/0	$Sr_2Bi_{3.5}La_{0.5}Ti_5O_{18}$	5.4629(9)	5.4617(9)	48.8178(18)	1456.6(3)
0.6/0	$Sr_2Bi_{3.4}La_{0.6}Ti_5O_{18}$	5.4576(10)	5.4586(10)	48.8137(30)	1454.2(4)
0.5/0.1	$Sr_2Bi_{3.47}La_{0.5}Ti_{4.9}Nb_{0.1}O_{18}$	5.4618(8)	5.4612(9)	48.7881(20)	1455.2(3)
0.5/0.2	$Sr_2Bi_{3.44}La_{0.5}Ti_{4.8}Nb_{0.2}O_{18}$	5.4643(7)	5.4646(7)	48.7660(14)	1456.1(3)
0.5/0.3	$Sr_2Bi_{3.41}La_{0.5}Ti_{4.7}Nb_{0.3}O_{18}$	5.4675(12)	5.4664(12)	48.7723(20)	1457.6(4)
0.5/0.4	$Sr_2Bi_{3.38}La_{0.5}Ti_{4.6}Nb_{0.4}O_{18}$	5.4676(9)	5.4664 (9)	48.8056(24)	1458.7(4)

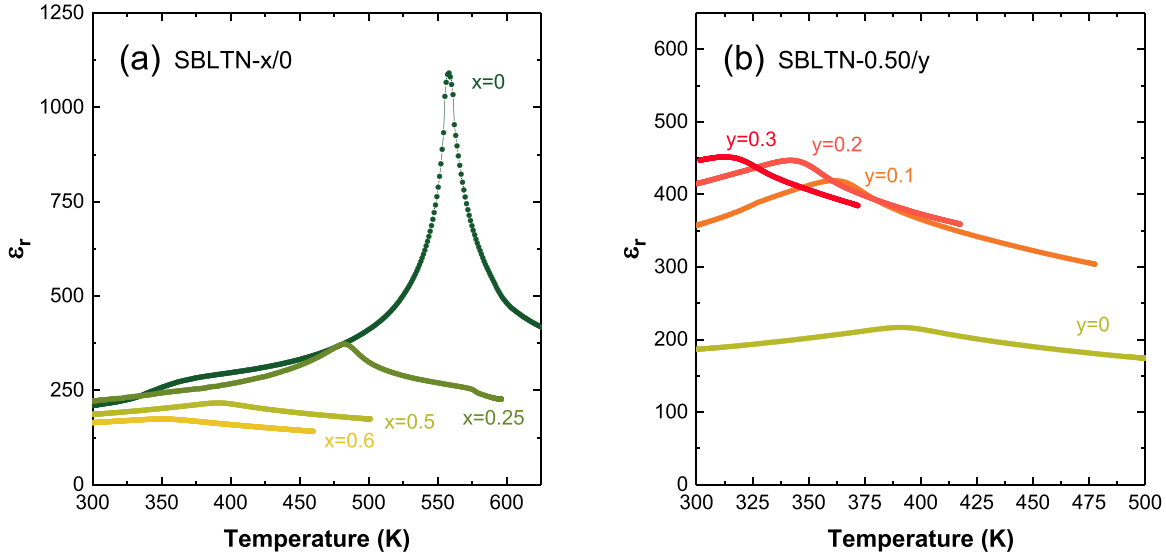

Fig. 3. Temperature dependence of the relative electric permittivity (ε_r) measured at 50 kHz frequency in heating runs for (a) SBLTN-$x/0$ ($x = 0$, 0.25, 0.5, 0.6) and (b) SBLTN-0.5/y ($y = 0$, 0.1, 0.2, 0.3, 0.4).

Table 2
Dielectric characteristic parameters for $Sr_2Bi_{4-x-1/3y}La_xTi_{5-y}Nb_yO_{18}$ (SBLTN-x/y) samples as derived from the relative electric permittivity εr measurements as a function of temperature. ε_m is the maximum value and T_m is the temperature at which $\varepsilon_r = \varepsilon_m$ derived from the heating runs at a frequency of 50 kHz. ΔT_m is the difference between the T_m values at 100 Hz and 100 kHz.

SBLTN-x/y	Composition	ε_m	T_m (K)	ΔT_m (K)
0/0	$Sr_2Bi_4Ti_5O_{18}$	1091	558	1
0.25/0	$Sr_2Bi_{3.75}La_{0.25}Ti_5O_{18}$	373	482	1
0.5/0	$Sr_2Bi_{3.5}La_{0.5}Ti_5O_{18}$	217	391	4
0.6/0	$Sr_2Bi_{3.4}La_{0.6}Ti_5O_{18}$	174	350	8
0.5/0.1	$Sr_2Bi_{3.47}La_{0.5}Ti_{4.9}Nb_{0.1}O_{18}$	419	361	4
0.5/0.2	$Sr_2Bi_{3.44}La_{0.5}Ti_{4.8}Nb_{0.2}O_{18}$	447	342	3
0.5/0.3	$Sr_2Bi_{3.41}La_{0.5}Ti_{4.7}Nb_{0.3}O_{18}$	451	313	2

ferroelectric properties are thus enhanced with the introduction of Nb in La doped SBLTN-0.5/0, which can be explained as follows. The decrease in the polarization of SBLTN-0/0 upon La doping must be related to the substitution of Bi^{3+} ($6s^2$) for an ion without lone pair such as La^{3+} and the concomitant lesser structural distortion because of its smaller size. Then, the significant recovery of polarization upon replacement of Ti^{4+} by Nb^{5+} can be primarily ascribed to the reduction of oxygen vacancies mediated by the excess electrons, as previously proposed for the related Aurivillius systems $Bi_{3.25}La_{0.75}Ti_{3-x}Nb_xO_{12}$ [30] and $SrBi_4Ti_{4-x}Nb_xO_{15}$ [21]. Oxygen vacancies are well-known to be the most mobile charges in perovskite ferroelectrics and act as space charge that causes strong domain pinning, yielding low intrinsic permittivity and polarization values [22,30].

In the following, we focus on the five-layer Aurivillius SBLTN-x/y compositions with optimum properties as EC materials for refrigeration applications near room temperature. Specifically, on the La/Nb codoped compounds SBLTN-0.5/y with $y = 0.2$ ($T_m \sim 342$ K) and $y = 0.3$ ($T_m \sim 313$ K), and their $P(E, T)$ curves at temperatures above and below T_m. Measurements are taken on heating from room temperature up to around 420 K, every 5–10 K, under E field amplitudes of about 40 kV/cm. Apart from the generally lower polarization values upon increasing Nb concentration from $y = 0.2$ to $y = 0.3$, the temperature dependence of the $P(E)$ curves is very similar. As illustrated in Figs. 6(a) and 6(b) for $y = 0.2$ and $y = 0.3$ compounds, respectively, the $P(E)$ loops become progressively slimmer upon warming, up to the typical paraelectric-like curve which does not fully close due to significant dielectric losses at high temperatures. Besides, P_r shows a rather sharp drop at T_m (Figs. 6(c) and 6(d)), also illustrated by the relatively narrow downward peak in the derivative, with a span of $\sim$ 25 K as deduced from the full width at half maximum for both $y = 0.2$ and $y = 0.3$ compositions. This behavior suggests diffuse rather than canonical relaxor behavior since the latter would not show a step-like drop [26]. Looking into the $P(E, T)$ curves in more detail, one can identify a sort of double or pinched hysteresis loop at temperatures well above T_m, for both compounds. The $P(E)$ curves at 390 K for $y = 0.2$ (Fig. 6(a)) and at 350 K for $y = 0.3$ (Fig. 6(b)) are representative of this behavior. Because the pinching is somewhat weak in our compounds, it is better appreciated in the current versus E field curves (Figs. S6 and S7), where the upward and downward peaks split from two to four and gradually faint upon warming. Pinched or double loops have been previously reported in perovskite-related systems and attributed to extrinsic (e.g., aging, defect-dipole pairs induced by non-stoichiometry) but also intrinsic mechanisms. An interesting theoretical study [37] proved the possibility of pinched loops in defect-free ferroelectrics with inhomogeneous dipolar pattern and recent

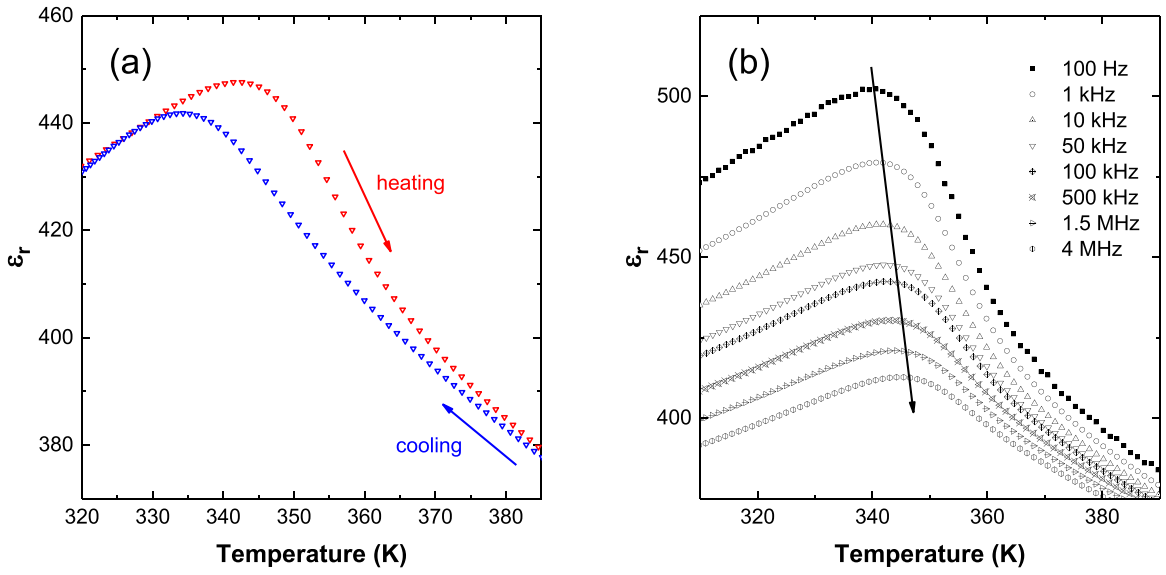

Fig. 4. Relative electric permittivity (ε_r) data for SBLTN-0.5/0.2. (a) Comparison between heating and cooling runs at 50 kHz. (b) Data measured while heating at several frequencies.

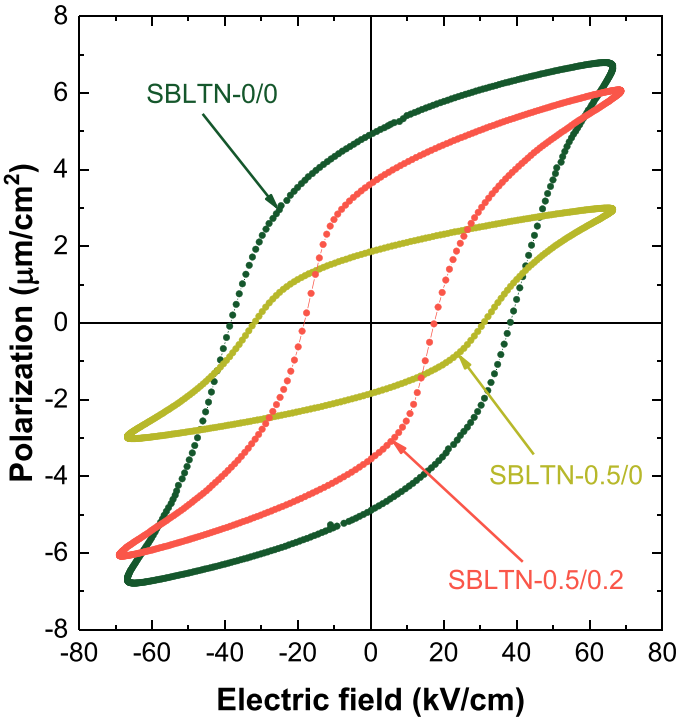

Fig. 5. Polarization versus electric field $P(E)$ curves at room temperature and 10 Hz frequency for SBLTN-0/0, SBLTN-0.5/0 and SBLTN-0.5/0.2.

Table 3
Ferroelectric hysteresis loop characteristic parameters for selected $Sr_2Bi_{4-x-1/3y}La_xTi_{5-y}Nb_yO_{18}$ (SBLTN-x/y) samples derived from the $P(E)$ curves measured at room temperature and 10 Hz frequency.

SBLTN-x/y	Composition	P_{max} (μC/cm^2)	P_r (μC/cm^2)	E_c (kV/cm)
0/0	$Sr_2Bi_4Ti_5O_{18}$	6.7	4.9	38.2
0.5/0	$Sr_2Bi_{3.5}La_{0.5}Ti_5O_{18}$	3.0	1.9	30.9
0.5/0.2	$Sr_2Bi_{3.44}La_{0.5}Ti_{4.8}Nb_{0.2}O_{18}$	6.1	3.6	17.4

experimental works are more and more discarding the extrinsic mechanisms. Very similar pinched loops were also reported for the relaxor Aurivillius phase $SrNaBi_2Nb_3O_{12}$ well above T_m and were attributed to the phase coexistence between non-polar and polar regions [38]. Another possibility for the origin of the pinched loop is an E-field-induced transition above T_m from short-range-ordered polar nanoregions (PNRs) to long-range ordered ferroelectric macrodomains, as reported for relaxor ceramics like $(Na_{0.5}Bi_{0.5})TiO_3$-based solid solutions [39] and $Pb_{0.91}La_{0.06}Zr_{0.8}Ti_{0.2}O_3$ [40]. Either way, the compositional disorder in our La/Nb codoped SBLTN-0.5/y compounds, including non-isovalent cations (Ti^{4+}, Nb^{5+}), yields a disordered matrix within which different ordered chemical nanoregions (i.e., the PNRs) are formed, which is also supported by the frequency dispersion of the electric permittivity, and would likely be at origin of the pinched $P(E)$ loops.

3.3. Electrocaloric properties

The ECE is determined as a function of temperature and at different E field variations, through both direct and indirect methods, for the La/Nb codoped compounds SBLTN-0.5/y ($y = 0.2$ and 0.3). We use a dedicated quasi-adiabatic calorimeter for the direct measurements, in which the temperature gradient between sample and cryostat (i.e., thermal bath) is collected continuously [33]. In a typical experiment, once stabilized the cryostat temperature, several voltage V values (given $E = V/d$, where d is the sample thickness) are applied in a multiple-pulse sequence. The E field is applied, the sample polarizes and increases its temperature because of the ECE (polarization, $\Delta T > 0$), then the field is fully removed (depolarization, $\Delta T < 0$), over a period of 100 seconds at each step. This E on/off sequence is repeated twice, therefore the whole evolution through time results in four temperature relaxations per each field variation $\Delta E = E - 0$ (Fig. S8). The adiabatic temperature change ΔT can be adequately extracted from the raw relaxation data by fitting them to an exponential decay, as previously described [33]. We find an excellent reproducibility (see Fig. S8), so that the average ΔT is given as the result. The ΔT values obtained for SBLTN-0.5/0.2 and SBLTN-0.5/0.3 show nicely defined peaks in the vicinity of T_m (Figs. 7(a) and 7(b)). We find that SBLTN-0.5/0.2 shows the maximum $\Delta T \sim 0.27$ K under $\Delta E = 37$ kV/cm, which occurs at a temperature of maximum ECE $T_{m,ECE} = 355$ K. Under this same field variation, ΔT reaches a more modest ~ 0.18 K in SBLTN-0.5/0.3, although the maximum moves closer to room temperature, being centered at $T_{m,ECE} = 325$ K. Besides, under this field

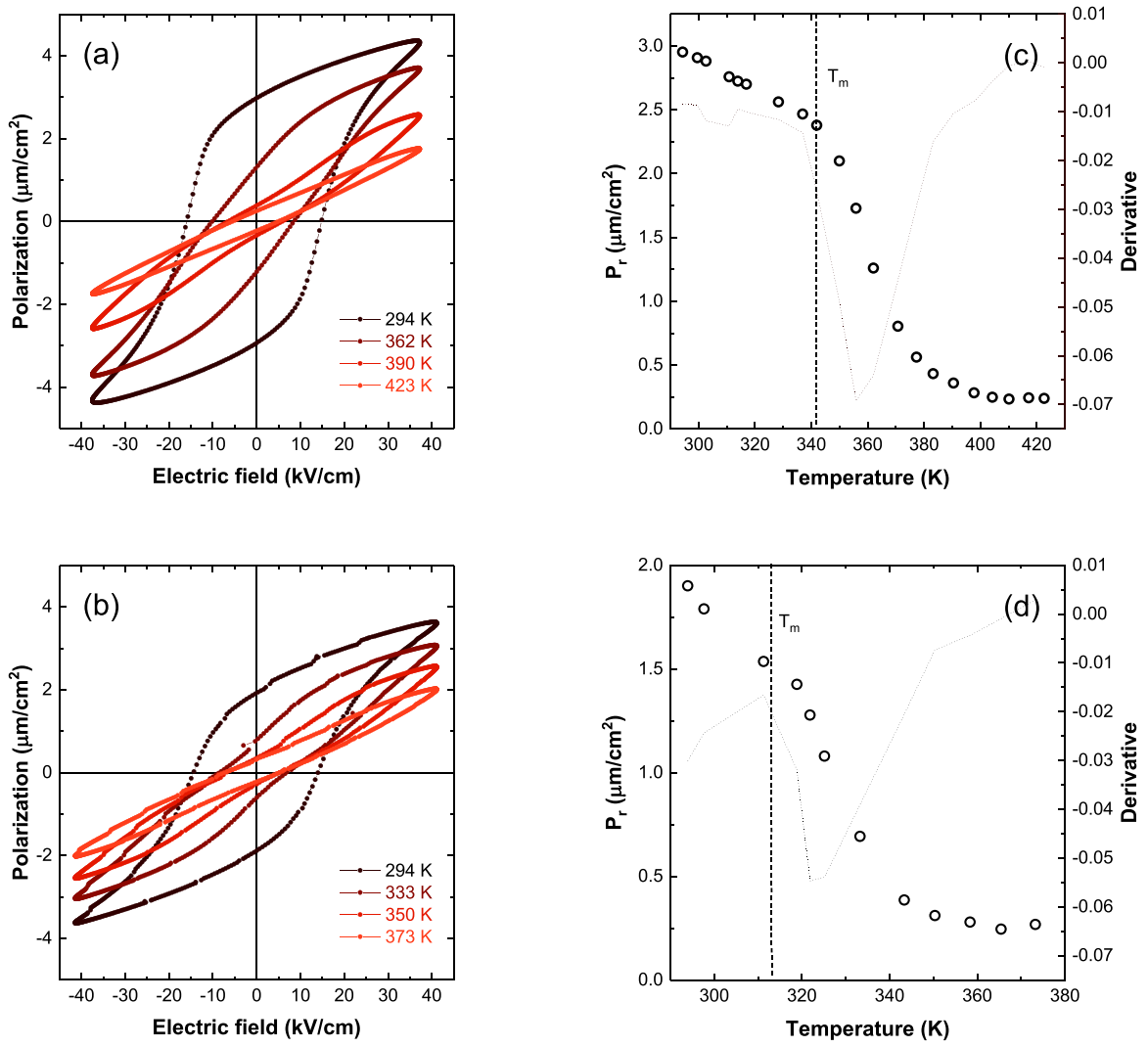

Fig. 6. Representative $P(E)$ curves measured on heating for (a) SBLTN-0.5/0.2 and (b) SBLTN-0.5/0.3 at 10 Hz. Evolution of the remanent polarization P_r as a function of temperature and its derivative (dotted line) for (c) SBLTN-0.5/0.2 and (d) SBLTN-0.5/0.3. The dashed (black) line indicates the position of T_m.

variation, the temperature span of the ECE $\Delta T_{span,ECE}$, i.e., the span corresponding to $\Delta T \geq 80\%$, is ~ 15 K for both $y = 0.2$ and $y = 0.3$ compositions. Direct ECE measurements were also performed for the $y = 0.4$ compound (Fig. S9), however this composition was not studied further as its ECE is significantly weaker and the maximum well below room temperature. In comparison with direct ECE measurements reported for other relaxor Aurivillius phases in bulk form, e.g., Pr-doped (T_m ~ 350 K) [18] and Ba-doped (T_m ~ 380 K) [19] $SrBi_2(Nb_{0.2}Ta_{0.8})_2O_9$, larger ΔT responses of ca. 0.4–0.8 K were obtained, although no well-defined ECE peaks were observed. We also note that, for SBLTN-0.5/y ($y = 0.2$ and 0.3), the temperature of maximum ECE $T_{m,ECE}$ shows a systematic shift towards higher values with increasing ΔE, i.e., it disperses with the E field. For the largest differences in ΔE variation, i.e., $\Delta T_{m,ECE}$ (4 kV/cm – 37 kV/cm) for $y = 0.2$ and $\Delta T_{m,ECE}$ (6 kV/cm – 37 kV/cm) for $y = 0.3$, we obtain considerable displacements ~ 13 K of the ECE maximum. A shift of the ECE peak upon increasing ΔE was reported before for conventional ferroelectric $BaTiO_3$ (although detected only for $\Delta T > 0$ data, i.e., E on, and not for $\Delta T < 0$, i.e., E off) [41] and also for relaxor bulk ceramics like $(Na_{0.5}Bi_{0.5})TiO_3$-based solid solutions [39], $Pb_{0.91}La_{0.06}Zr_{0.8}Ti_{0.2}O_3$ [40] and $Ba_{1-y}Ca_yTi_{1-x}Hf_xO_3$ [33], with different magnitudes in each case. Similarly, an inverse shift of the ECE peak was recently found in a thin film of four-layered perovskite $Bi_5Ti_3AlO_{15}$ with giant negative ECE [42]. Theoretical studies predict this behavior to occur in relaxor ferroelectrics showing field-induced first-order transitions [43]. Therefore, the large shifts in the ECE maximum exhibited by SBLTN-0.5/y ($y = 0.2$ and 0.3), suggest that the dominant contribution are E-field-induced transitions well above T_m from the diffuse relaxor ferroelectric state with short-range-ordered PNRs to a ferroelectric state with long-range order.

Next, we also estimate ΔT indirectly by applying thermodynamic formulations to the $P(E, T)$ curves measured at several temperatures above and below T_m. Only the upper branch with $E > 0$ is used for the indirect calculation as recommended in previous works [11,41]. An eighth-order polynomial is fitted to the isothermal $P(E, T)$ curves so that all their data points occur at the same E field values and then transpose $P(E)$ at the set of measured T values to give $P(T)$ at the new set of E values. Then, the derivative of P with respect to temperature is calculated from the small experimental incremental values of polarization versus temperature (5–10 K steps) at a given E value, and finally the analysis is completed through stepwise integration to derive the entropy variation of the ECE, namely,

$$\Delta S = -\int_0^E \left(\frac{\partial P}{\partial T}\right)_{E'} dE', \quad (1)$$

for any field change $\Delta E = E - 0$ as it is our case. The adiabatic temperature variation ΔT can be calculated as well, namely,

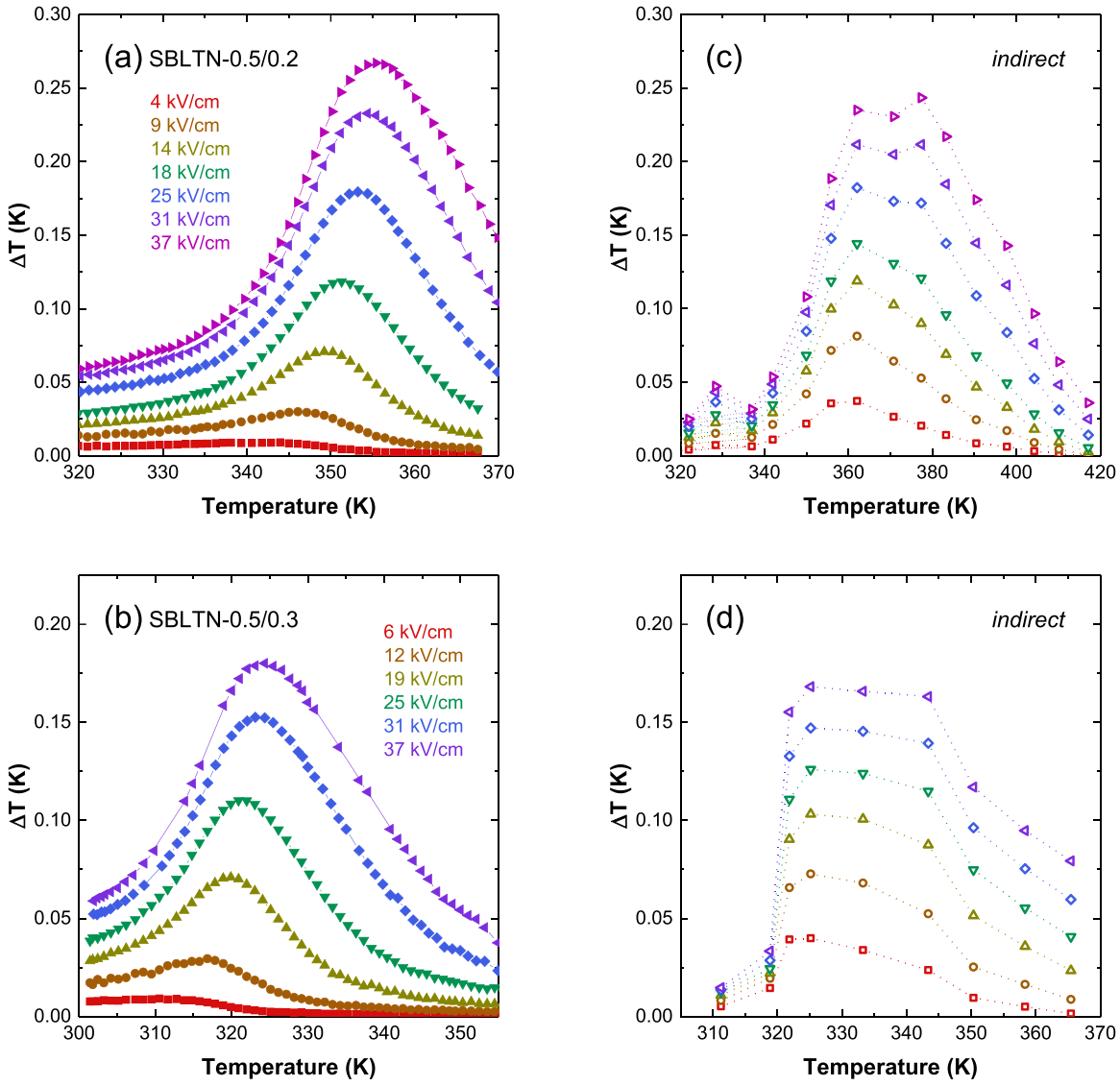

Fig. 7. Direct measurements of the ECE adiabatic temperature change ΔT for (a) SBLTN-0.5/0.2 and (b) SBLTN-0.5/0.3, together with its indirect derivation in (c) and (d) respectively, as a function of temperature at different electric field variations ΔE.

$$\Delta T = -\frac{1}{\rho}\int_0^E \frac{T(E)}{c_p(E)}\left(\frac{\partial P}{\partial T}\right)_{E'} dE', \tag{2}$$

where ρ is the density and c_p the heat capacity of the material [11]. As generally applied for practical indirect ΔT calculations, both T and c_p are assumed E independent. Thus, Eq. (2) can be simplified as

$$\Delta T \approx -\frac{T}{\rho c_p}\Delta S. \tag{3}$$

Regarding the density, we determined $\rho = 6.32$ g cm^{-3} (SBLTN-0.5/0.2) and $\rho = 6.24$ g cm^{-3} (SBLTN-0.5/0.3) using the Archimedes' method, while the theoretical values as deduced using the refined lattice parameters from the XRD data, are $\rho_{XRD} = 6.84$ g cm^{-3} (SBLTN-0.5/0.2) and $\rho_{XRD} = 6.82$ g cm^{-3} (SBLTN-0.5/0.3). This means that our ceramic samples reached relative densities $> 91\%$ and were thus well sintered. Heat capacity measurements (Fig. S10) revealed no marked differences between the SBLTN-0.5/0.2 and SBLTN-0.5/0.3 compositions, being c_p weakly temperature dependent between 300 and 400 K, that is, no anomalies attributable to conventional ferroelectric transitions were detected, consistently with the diffuse relaxor ferroelectric character [26]. Considering $c_p = 0.42$ J g^{-1} K^{-1} for both SBLTN-0.5/0.2 and SBLTN-0.5/0.3 compositions, in addition to the corresponding experimental density values, we have calculated ΔT from Eq. (3) for ΔE variations matching the direct measurements. As shown in Figs. 7(c) and 7(d), a qualitative agreement between direct and indirect methods is obtained for the surveyed SBLTN-x/y compositions. A well-defined peak is also observed in the indirectly estimated $\Delta T(T)$ curves that gradually grows in intensity when increasing the E field. For the largest E field value, the indirect results correctly predict ΔT values greater in $y = 0.2$ than in $y = 0.3$, while the magnitudes do not perfectly coincide with the direct values. Besides, the rate of the ECE enhancement with the field is not well captured in the indirect estimations and the peaks are substantially much broader than in the direct ECE measurements. Similar disagreements were also found in other works dealing with relaxor ferroelectrics [33,39,40]. The problem is that Maxwell relations assume thermal equilibrium which does not hold for relaxor ferroelectrics with PNRs having different relaxation times [11]. Hence, the application of indirect methods based on Maxwell relations is limited to a qualitative prediction of the ECE in relaxors and must be used with caution, ideally contrasted with direct measurements.

4. Conclusions

We have investigated the EC potential of five-layer Aurivillius phase $Sr_2Bi_4Ti_5O_{18}$ upon La and Nb codoping through a comprehensive characterization of the structural and electrical properties, and direct jointly with indirect measurements of the ECE. The new, lead-free, five-layer Aurivillius compounds $Sr_2Bi_{4-x-1/3y}La_xTi_{5-y}Nb_yO_{18}$ (SBLTN-x/y), that further sub-divide into La-doped SBLTN-$x/0$ ($0 \leq x \leq 0.6$) and La/Nb codoped SBLTN-0.5/y ($0.1 \leq y \leq 0.4$) series; are successfully prepared by the standard solid-state reaction method and they all adopt the orthorhombic crystal structure of the parent compound. Electric permittivity and polarization measurements confirm the suitability of the strategy based on La/Nb codoping in $Sr_2Bi_4Ti_5O_{18}$ ($T_C \sim 560$ K) for decreasing the transition temperature while maintaining reasonable ferroelectric properties. Adding Nb doping to the moderate La-doped composition compound SBLTN-0.5/0 ($T_m \sim 391$ K), allows decreasing further T_m in the SBLTN-0.5/y series ($T_m \sim 342$ K for $y = 0.2$ and $T_m \sim 313$ K for $y = 0.3$) while enhancing the electric permittivity and polarization, besides reducing the coercive field. In addition, La/Nb codoped SBLTN-0.5/y compounds exhibit some peculiarities in the temperature dependence of the electric permittivity and polarization. The permittivity results show a significant thermal hysteresis and a frequency dispersion in agreement with a modest relaxor behaviour. In the $P(E, T)$ curves, the remanent polarization shows a rather sharp drop at T_m and, well above this temperature, pinched polarization loops are detected with a clearly defined double peak in the current versus field data that can be attributed to field-induced transitions from short-range-ordered PNRs to long-range ordered ferroelectric macrodomains typical of diffuse relaxor systems.

Regarding the ECE measurements, our direct results in a dedicated quasi-adiabatic calorimeter have provided very well-defined peaks of the adiabatic temperature change as a function of temperature $\Delta T(T)$ in the proximity of T_m that strongly shift upon increasing the E field variation, a behavior previously reported for relaxor ferroelectrics in both experimental [33,39,40,42] and theoretical [43] works. SBLTN-0.5/0.2 composition shows the best EC performance with a maximum $\Delta T \sim 0.3$ K at 355 K and temperature span $\sim$ 15 K, under $\Delta E = 37$ kV/cm, while the optimum composition in terms the closest proximity of the ECE to room temperature is SBLTN-0.5/0.3, with a maximum $\Delta T \sim 0.2$ K at 325 K and temperature span $\sim$ 16 K, under the same ΔE. We have also evaluated the indirect estimations of the ECE by standard and commonly applied thermodynamic analysis of the $P(E, T)$ data based on Maxwell relations. While a maximum is clearly discerned in the indirect estimations of $\Delta T(T)$, neither the intensity variation upon increasing ΔE nor the temperature span, are well reproduced with respect to the direct measurements. Because relaxor ferroelectrics are an important class of potential EC materials with interesting characteristics like broad temperature spans and large E field dispersion of the ECE, direct measurements are thus the only reliable technique for evaluating their performance. Following the promising results of a tunable ECE in bulk La/Nb codoped $Sr_2Bi_4Ti_5O_{18}$ in the vicinity of room temperature, a future direction for improving further the EC performance in these materials would be the preparation of the best compositions in the form of thin films.

Declaration of Competing Interest

The authors declare that they have no known competing financial interests or personal relationships that could have appeared to influence the work reported in this paper.

Data Availability

Data are available at https://digital.csic.es/handle/10261/336892.

Acknowledgments

The authors are grateful to E. Palacios for discussions on the calorimetric measurements. S. L. acknowledges funding from the European Union's Horizon 2020 research and innovation program under the Marie Skłodowska-Curie grant agreement No. 101029019. This work was also supported by Ministerio de Ciencia, Innovación y Universidades (PID2021-124734OB-C21) and Diputación General de Aragón (E11-23R, E12-23R). D. G. acknowledges financial support from the Gobierno de Aragón through a doctoral fellowship. Authors would also like to acknowledge Servicio General de Apoyo a la Investigación from Universidad de Zaragoza and Unidad Técnica en Ingeniería de Microdispositivos from INMA.

Appendix A. Supporting information

Supplementary data associated with this article can be found in the online version at doi:10.1016/j.jallcom.2024.173923.

Supplementary Material See Supplementary Material for: XRD data and Rietveld refinements for SBLTN-0/0, SBLTN-0.5/0, SBLTN-0.5/0.2 and SBLTN-0.5/0.3 (Fig. S1- Fig. S4); $P(E)$ curves at room temperature for SBLTN-$x/0$ where $x = 0$, 0.25, 0.5, 0.6 and SBLTN-0.5/y where $y = 0$, 0.1, 0.2 (Fig. S5); polarization and current-versus-electric-field curves at selected temperatures for SBLTN-0.5/y with $y = 0.2$ (Fig. S6) and $y = 0.3$ (Fig. S7); a representative raw direct measurement of the ECE for SBLTN-0.5/0.2 (Fig. S8), direct measurements of the ECE for SBLTN-0.5/0.4 (Fig. S9); and heat capacity measurements for SBLTN-0.5/y ($y = 0.2$ and 0.3) (Fig. S10).

References

[1] I. Takeuchi, K. Sandeman, Solid-state cooling with caloric materials, Phys. Today 68 (2015) 48–54, https://doi.org/10.1063/PT.3.3022.
[2] X. Moya, N.D. Mathur, Caloric materials for cooling and heating, Science 370 (80) (2020) 797–803, https://doi.org/10.1126/science.abb0973.
[3] X. Moya, E. Defay, V. Heine, N.D. Mathur, Too cool to work, Nat. Publ. Gr. 11 (2015) 202, https://doi.org/10.1038/nphys3271.
[4] J. Shi, D. Han, Z. Li, L. Yang, S.G. Lu, Z. Zhong, J. Chen, Q.M. Zhang, X. Qian, Electrocaloric cooling materials and devices for zero-global-warming-potential, high-efficiency refrigeration, Joule 3 (2019) 1200–1225, https://doi.org/10.1016/j.joule.2019.03.021.
[5] M. Otoničar, B. Dkhil, Electrocalorics hit the top, Nat. Mater. 19 (2020) 9–11, https://doi.org/10.1038/s41563-019-0522-1.
[6] M. Ožbolt, A. Kitanovski, J. Tušek, A. Poredoš, Electrocaloric refrigeration: thermodynamics, state of the art and future perspectives, Int. J. Refrig. 40 (2014) 174–188, https://doi.org/10.1016/j.ijrefrig.2013.11.007.
[7] J.F. Scott, Electrocaloric materials, Annu. Rev. Mater. Res. 41 (2011) 229–240, https://doi.org/10.1146/annurev-matsci-062910-100341.
[8] X. Moya, S. Kar-Narayan, N.D. Mathur, Caloric materials near ferroic phase transitions, Nat. Mater. 13 (2014) 439–450, https://doi.org/10.1038/nmat3951.
[9] M. Valant, Electrocaloric materials for future solid-state refrigeration technologies, Prog. Mater. Sci. 57 (2012) 980–1009, https://doi.org/10.1016/j.pmatsci.2012.02.001.
[10] T. Correia, Q. Zhang, Electrocaloric Materials, Springer Berlin Heidelberg, Berlin, Heidelberg, 2014, https://doi.org/10.1007/978-3-642-40264-7.
[11] Y. Liu, J.F. Scott, B. Dkhil, Direct and indirect measurements on electrocaloric effect: Recent developments and perspectives, Appl. Phys. Rev. 3 (2016), https://doi.org/10.1063/1.4958327.
[12] B.H. Park, B.S. Kang, S.D. Bu, T.W. Noh, J. Lee, W. Jo, Lanthanum-substituted bismuth titanate for use in non-volatile memories, Nature 401 (1999) 682–684, https://doi.org/10.1038/44352.
[13] C.A.-P. de Araujo, J.D. Cuchiaro, L.D. McMillan, M.C. Scott, J.F. Scott, Fatigue-free ferroelectric capacitors with platinum electrodes, Nature 374 (1995) 627–629, https://doi.org/10.1038/374627a0.

[14] H. Chen, T.L. Ren, X.M. Wu, Y. Yang, L.T. Liu, Giant electrocaloric effect in lead-free thin film of strontium bismuth tantalite, Appl. Phys. Lett. 94 (2009) 67–70, https://doi.org/10.1063/1.3123817.
[15] J. Zhu, W.-P. Lu, X.-Y. Mao, R. Hui, X.-B. Chen, Study on properties of lanthanum doped SrBi 4 Ti 4 O 15 and Sr 2 Bi 4 Ti 5 O 18 ferroelectric ceramics, Jpn. J. Appl. Phys. 42 (2003) 5165–5168, https://doi.org/10.1143/JJAP.42.5165.
[16] F. Qiang, J.H. He, J. Zhu, X.B. Chen, Ferroelectric and dielectric properties of bismuth-layered structural Sr2Bi4-xLnxTi5O18 (Ln=La, Nd, Sm and Dy) ceramics, J. Solid State Chem. 179 (2006) 1768–1774, https://doi.org/10.1016/j.jssc.2006.03.012.
[17] F. Le Goupil, Electrocaloric effect in ferroelectric relaxors: The road to solid-state cooling, 2013.
[18] A.K. Axelsson, F. Le Goupil, M. Valant, N.M.N. Alford, Electrocaloric effect in lead-free Aurivillius relaxor ferroelectric ceramics, Acta Mater. 124 (2017) 120–126, https://doi.org/10.1016/j.actamat.2016.11.001.
[19] A.K. Axelsson, F. Le Goupil, M. Valant, N.M.N. Alford, Optimisation of SrBi2(Nb, Ta)2O9 Aurivillius phase for lead-free electrocaloric cooling, J. Eur. Ceram. Soc. 38 (2018) 5354–5358, https://doi.org/10.1016/j.jeurceramsoc.2018.07.044.
[20] M. Kashyap, V. Shrivastava, R. Mishra, Twin-peak electrocaloric effect in ferroelectric phase of diffusive SrBi1.98La0.02Nb2?xTaxO9 materials, Phys. Status Solidi Basic Res. 258 (2021) 2100266, https://doi.org/10.1002/pssb.202100266.
[21] R. Jose, P. Vineetha, M.A. Rafiq, K. Venkata Saravanan, Investigation into defect chemistry and relaxation processes in niobium doped and undoped SrBi4Ti4O15 using impedance spectroscopy, RSC Adv. 8 (2018) 34437–34448, https://doi.org/10.1039/c8ra06621c.
[22] W.P. Lu, R. Hui, X.B. Chen, Defect structure in undoped and donor-doped polycrystalline Sr 2Bi4Ti5O18, Integr. Ferroelectr. 65 (2004) 97–103, https://doi.org/10.1080/10584580490892863.
[23] F. Le Goupil, J. Bennett, A. Axelsson, M. Valant, A. Berenov, A.J. Bell, P. Tim, N. M. Alford, F. Le Goupil, J. Bennett, A. Axelsson, M. Valant, Electrocaloric enhancement near the morphotropic phase boundary in lead-free NBT- KBT ceramics, 172903, Appl. Phys. Lett. (2015) 1–5, https://doi.org/10.1063/1.4934759.
[24] F. Le Goupil, R. McKinnon, V. Koval, G. Viola, S. Dunn, A. Berenov, H. Yan, N.M. N. Alford, Tuning the electrocaloric enhancement near the morphotropic phase boundary in lead-free ceramics, Sci. Rep. 6 (2016) 3–8, https://doi.org/10.1038/srep28251.
[25] V.V. Shvartsman, D.C. Lupascu, Lead-free relaxor ferroelectrics, J. Am. Ceram. Soc. 95 (2012) 1–26, https://doi.org/10.1111/j.1551-2916.2011.04952.x.
[26] A.A. Bokov, Z. Ye, Recent progress in relaxor ferroelectrics with perovskite structure, 1 (2006) 31–52. ⟨https://doi.org/10.1007/s10853-005-5915-7⟩.
[27] K. Momma, F. Izumi, VESTA 3 for three-dimensional visualization of crystal, volumetric and morphology data, J. Appl. Crystallogr. 44 (2011) 1272–1276, https://doi.org/10.1107/S0021889811038970.
[28] P. Ferrer, M. Algueró, J.E. Iglesias, A. Castro, Processing and dielectric properties of Bi4Srn−3TinO3n+3 (n=3, 4 and 5) ceramics obtained from mechanochemically activated precursors, J. Eur. Ceram. Soc. 27 (2007) 3641–3645, https://doi.org/10.1016/j.jeurceramsoc.2007.02.005.
[29] X.B. Chen, R. Hui, J. Zhu, W.P. Lu, X.Y. Mao, Relaxor properties of lanthanum-doped bismuth layer-structured ferroelectrics, J. Appl. Phys. 96 (2004) 5697–5700, https://doi.org/10.1063/1.1807029.
[30] J.H. Park, J.S. Bae, B.C. Choi, J.H. Jeong, Effect of Nb doping of ferroelectric properties of Bi 3.25 La 0.75 Ti 3 O 12 ceramics, J. Appl. Phys. 97 (2005) 2–6, https://doi.org/10.1063/1.1862318.
[31] H. Du, L. Tang, S. Kaskel, Preparation, Microstructure, and ferroelectric properties of Bi 3.25 La 0.75 Ti 3− x M x O 12 (M = Mo, W, Nb, V) ceramics, J. Phys. Chem. C 113 (2009) 1329–1339, https://doi.org/10.1021/jp809130v.
[32] J. Rodriguez-carvajal, Recent advances in magnetic structure determination by neutron powder diffraction, Phys. B Condens. Matter 192 (1993) 55–69, https://doi.org/10.1016/0921-4526(93)90108-I.
[33] D. Gracia, S. Lafuerza, J. Blasco, M. Evangelisti, The electrocaloric effect of lead-free Ba1− y Ca y Ti1− x Hf x O3 from direct and indirect measurements, APL Mater. 11 (2023) 121101, https://doi.org/10.1063/5.0173585.
[34] Ismunandar, T. Kamiyama, A. Hoshikawa, Q. Zhou, B.J. Kennedy, Y. Kubota, K. Kato, Structural studies of five layer Aurivillius oxides: A 2Bi 4Ti 5O 18 (A=Ca, Sr, Ba and Pb), J. Solid State Chem. 177 (2004) 4188–4196, https://doi.org/10.1016/j.jssc.2004.07.032.
[35] B.Y.R.D. Shannon, M. H, N.H. Baur, O.H. Gibbs, M. Eu, V. Cu, Revised effective ionic radii and systematic studies of interatomie distances in halides and chaleogenides central research and development department, experimental station, E. L Du Pont de Nemours the effective ionic radii of Shannon & Prewitt [Acta], Acta Crystallogr. Sect. A. 32 (1976) 751, https://doi.org/10.1107/S0567739476001551.
[36] Y. González-Abreu, A. Peláiz-Barranco, J.D.S. Guerra, Y. Gagou, P. Saint-Grégoire, From normal ferroelectric transition to relaxor behavior in Aurivillius ferroelectric ceramics, J. Mater. Sci. 49 (2014) 7437–7444, https://doi.org/10.1007/s10853-014-8448-0.
[37] B. Xu, C. Paillard, B. Dkhil, L. Bellaiche, Pinched hysteresis loop in defect-free ferroelectric materials, Phys. Rev. B 94 (2016) 1–5, https://doi.org/10.1103/PhysRevB.94.140101.
[38] S. Kumar, D.A. Ochoa, J.E. García, K.B.R. Varma, Relaxor ferroelectric behavior and structural aspects of SrNaBi2Nb3O12 ceramics, J. Am. Ceram. Soc. 95 (2012) 1339–1342, https://doi.org/10.1111/j.1551-2916.2011.04954.x.
[39] X. Su, R. Yin, Y. Hou, J. Li, J. Li, S. Qin, Y. Su, L. Qiao, C. Liu, Y. Bai, Non-ergodic – ergodic transition and corresponding electrocaloric effect in lead-free bismuth sodium titanate-based relaxor ferroelectrics, J. Eur. Ceram. Soc. 42 (2022) 4917–4925, https://doi.org/10.1016/j.jeurceramsoc.2022.05.024.
[40] J. Li, J. Li, S. Qin, X. Su, L. Qiao, Y. Wang, T. Lookman, Y. Bai, Effects of long- and short-range ferroelectric order on the electrocaloric effect in relaxor ferroelectric ceramics, Phys. Rev. Appl. 11 (2019) 1, https://doi.org/10.1103/PhysRevApplied.11.044032.
[41] X. Moya, E. Stern-Taulats, S. Crossley, D. González-Alonso, S. Kar-Narayan, A. Planes, L. Mañosa, N.D. Mathur, Giant electrocaloric strength in single-crystal BaTiO3, Adv. Mater. 25 (2013) 1360–1365, https://doi.org/10.1002/adma.201203823.
[42] Y. Li, W. Lin, B. Yang, F. Guo, S. Zhao, Giant negative electrocaloric effect over an ultra-wide temperature region in relaxation frozen state ferroelectrics, ACS Appl. Mater. Interfaces 14 (2022) 53007–53018, https://doi.org/10.1021/acsami.2c17139.
[43] R. Pirc, Z. Kutnjak, R. Blinc, Q.M. Zhang, Electrocaloric effect in relaxor ferroelectrics, 074113 (2011) 1–7. ⟨https://doi.org/10.1063/1.3650906⟩.